Nonlinear Dynamics manuscript No.
(will be inserted by the editor)

Classification of the bifurcation structure of a periodically driven gas bubble

Roxána Varga · **Ferenc Hegedűs**

Received: date / Accepted: date

Abstract The bifurcation structure of a periodically driven spherical gas/vapour bubble is examined by means of methods of nonlinear analysis. The study of Behnia and his co-workers [1] revealed that the bifurcation structures with the pressure amplitude of the excitation as control parameter are structurally similar provided that $R_E\omega$ is kept constant. In the present paper, this problem is revisited. Analytical and numerical investigations of the bubble oscillator, which is the Keller–Miksis equation, are presented. It is shown that the validity range of Behnia's condition is governed by the viscosity and the surface tension, and holds only for relatively large bubbles. In water, the effect of viscosity is negligible, and the surface tension plays significant role at bubble size lower than approximately $5\,\mu$m.

Keywords Bubble dynamics · Bifurcation structure · Topology · Keller-Miksis equation · Nonlinear dynamics

1 Introduction

The radial oscillation of a periodically excited gas/vapour bubble is known to be strongly nonlinear. In the past century, many researchers devoted their attention to the dynamics of such bubbles. They are noteworthy not only from theoretical point of view but also due to the phenomena and their corresponding applications associated with them as well.

Irradiating a liquid domain with high frequency high amplitude ultrasound (periodic driving), micron-sized bubbles may develop forming bubble clusters [2–4]. Their radial pulsation can be so violent that at the minimum radius, the temperature and pressure inside the bubble can reach thousands of Kelvin and bar, respectively. This phenomenon is known

R. Varga
Department of Hydrodynamic Systems
Faculty of Mechanical Engineering
Budapest University of Technology and Economics
Tel.: +36 1 463-3097
E-mail: rvarga@hds.bme.hu

F. Hegedűs
Department of Hydrodynamic Systems
Faculty of Mechanical Engineering
Budapest University of Technology and Economics

as the bubble collapse. The generated extreme conditions are exploited by many industrial applications including sonochemistry [5–10], food processing [11–13] or even medical treatment [14–17].

As the size of the literature of experimental research is continuously growing, so is the number of theoretical and numerical papers on the topic of bubble oscillation. The accumulated knowledge of this nonlinear behavior has been summarized in many reviews [18–20] and papers [1, 21–36]. The most important findings are the existence of period-doubling cascades in the bifurcation structure [1, 21, 30, 31, 35], the appearance of resonance horns in the amplitude–frequency plane of the driving [24, 27, 34] or the alternation of chaotic and periodic windows [21, 23, 33]. These structures show similarities with the results obtained on other nonlinear oscillators such as Toda [37], Duffing [38–41] and others [42], implying that they are universal features of nonlinear systems rather than unique properties of oscillating bubbles.

The results of Behnia et al. [1], however, is a specialty of nonlinear bubble dynamics. They found that the bifurcation structures of different pressure amplitude response curves are remarkably similar when $R_E\omega$ is kept constant, but detailed physical explanation and range of validity was omitted. Here R_E is the equilibrium radius (size of the bubble) and ω is the excitation frequency of the periodic driving. Later Hegedűs et. al. [27], using the Rayleigh–Plesset equation, pointed out that almost all the parameters of the dimensionless form of the equation with constant $R_E\omega$ remain constant as well. Therefore, the bifurcation structure should not change drastically either. In the present paper, this problem is revisited using the same equation, the Keller–Miksis oscillator, as applied by Behnia et al. [1]. The detailed analytical and numerical investigations revealed the range of the applicability of Behnia's condition, which is affected by the viscosity and the surface tension. In case of water, the influence of the viscosity is negligible while the effect of surface tension becomes important at bubble size lower than $5\,\mu$m.

2 The bubble oscillator

To describe the time evolution of the bubble radius $R(t)$ in liquid water, a slightly modified form [18] of the well-known Keller–Miksis equation [43] was used:

$$\left(1-\frac{\dot{R}}{c_L}\right)R\ddot{R}+\left(1-\frac{\dot{R}}{3c_L}\right)\frac{3}{2}\dot{R}^2=$$
$$\frac{1}{\rho_L}\left(1+\frac{\dot{R}}{c_L}\right)(p_L-p_\infty(t))+\frac{R}{\rho_L c_L}\frac{d\,(p_L-p_\infty(t))}{dt}. \tag{1}$$

This equation assumes spherical bubble and takes into account the compressibility of the liquid domain, thus it incorporates sound radiation. The dot stands for the derivative with respect to time. ρ_L and c_L are the density and sound speed of the liquid, respectively. The pressure at the bubble wall is p_L while the pressure far away from the bubble is

$$p_\infty = P_\infty + p_A\sin(\omega t), \tag{2}$$

where P_∞ is the static or ambient pressure, p_A is the pressure amplitude and ω is the angular frequency of the periodic excitation.

The relationship between the pressures inside and outside the bubble at the bubble wall can be written as

$$p_G + p_V = p_L + \frac{2\sigma}{R} + 4\mu_L\frac{\dot{R}}{R}, \tag{3}$$

Table 1 Liquid properties calculated at $T_\infty = 25\,^{\circ}\mathrm{C}$ and at $P_\infty = 1\,\mathrm{bar}$ by means of the Haar–Gallagher–Kell equation of state [44].

parameter	value [unit]
p_V	3166.8 [Pa]
σ	0.0720 [N/m]
μ_L	0.00089 [kg/ms]
ρ_L	997.064 [kg/m^3]

where the total pressure inside the bubble is the sum of the partial pressures of the non-condensable gas content p_G and the vapour pressure p_V. The surface tension is σ and the liquid kinematic viscosity is μ_L. The gas inside the bubble obeys a simple polytropic relationship:

$$p_G = p_{g0}\left(\frac{R_0}{R}\right)^{3n}, \tag{4}$$

where p_{g0} and R_0 are the gas reference pressure and radius, respectively. Assuming adiabatic state of change and diatomic molecules of the gas content, the polytropic exponent is set to $n = 1.4$.

2.1 Parameters of the system

During the computations, the ambient pressure $P_\infty = 1\,\mathrm{bar}$ and the ambient temperature $T_\infty = 25\,^{\circ}\mathrm{C}$ were constants. These quantities specify all the liquid material properties, which were determined by means of the Haar–Gallagher–Kell equation of state [44]. The values of the material properties for water are listed in Table 1.

The bubble size is defined by the equilibrium radius R_E of the unexcited system, which is governed by the static mechanical balance at the gas-liquid interface:

$$0 = p_{g0}\left(\frac{R_0}{R_E}\right)^{3n} + p_V - P_\infty - \frac{2\sigma}{R_E}. \tag{5}$$

The reference pressure p_{g0} and reference radius R_0 can be arbitrarily chosen. In this study, the equilibrium radius R_E is the main control parameter. Therefore, if R_0 is set to be the equilibrium radius R_E, than the reference pressure can be determined from Eq. (5):

$$p_{g0} = \frac{2\sigma}{R_E} - (p_V - P_\infty). \tag{6}$$

Finally, the pressure amplitude p_A and the excitation frequency ω of the harmonic forcing are regarded as secondary control parameters.

2.2 The dimensionless equation system

For the numerical simulations, Eqs. (1)-(4) need to be rewritten into a first order dimensionless differential equation system. By the introduction of dimensionless time $\tau = t\omega/2\pi$,

dimensionless bubble radius $y_1 = R/R_E$ and bubble wall velocity $y_2 = 2\pi\dot{R}/R_E\omega$, the system can be written as

$$\begin{aligned} y_1' &= y_2, \\ y_2' &= \frac{N}{D}, \end{aligned} \tag{7}$$

where $'$ denotes the derivative with respect to τ. The numerator N is defined as

$$\begin{aligned} N = \frac{(p_L - p_\infty)}{p_{ref} y_1} + \frac{y_2}{\mu^A_{ref} y_1}\left(p_G(1-3n) - p_\infty(\tau) + p_V\right) \\ - \frac{p_A \cos(2\pi\tau)}{\mu^B_{ref}} - \left(1 - \frac{M}{3}\right)\frac{3}{2}\frac{y_2^2}{y_1} \end{aligned} \tag{8}$$

and the denominator D is

$$D = 1 - M + \frac{4\mu_L}{\mu_{ref} y_1}. \tag{9}$$

The parameters in Eqs. (8) and (9) are defined as follows. The reference pressure is

$$p_{ref} = \rho_L R_E^2 \left(\frac{\omega}{2\pi}\right)^2. \tag{10}$$

The reference viscosities are

$$\mu_{ref} = c_L \rho_L R_E, \tag{11}$$

$$\mu^A_{ref} = c_L \rho_L R_E \frac{\omega}{2\pi} = \mu_{ref}\frac{\omega}{2\pi}, \tag{12}$$

$$\mu^B_{ref} = c_L \rho_L R_E \frac{\omega}{(2\pi)^2} = \mu^A_{ref}\frac{1}{2\pi}. \tag{13}$$

The Mach number is

$$M = \frac{R_E \omega y_2}{2\pi c_L}. \tag{14}$$

The gas pressure inside the bubble becomes

$$p_G = \left(\frac{2\sigma}{R_E} - (p_V - P_\infty)\right)\left(\frac{1}{y_1}\right)^{3n}. \tag{15}$$

The pressure in the liquid domain at the bubble wall and the pressure far away from the bubble are

$$p_L = p_G + p_V - \frac{2\sigma}{R_E y_1} - 4\mu_L \frac{\omega}{2\pi}\frac{y_2}{y_1} \tag{16}$$

and

$$p_\infty(\tau) = P_\infty + p_A \sin(2\pi\tau), \tag{17}$$

respectively.

Since the angular frequency can vary on a scale of many orders of magnitude, it is reasonable to normalize it with a suitable reference quantity. Therefore, a dimensionless relative frequency was used for the computations defined as

$$\omega_f = \frac{\omega}{\omega_0}, \tag{18}$$

where ω_0 is the linear resonant frequency of the system. According to Brennen [45], ω_0 can be calculated from the following equation:

$$\omega_0 = \sqrt{\frac{3n(P_\infty - p_v)}{\rho_L R_E^2} + \frac{2(3n-1)\sigma}{\rho_L R_E^3} - \frac{4\mu_L^2}{\rho_L^2 R_E^4}}. \tag{19}$$

2.3 Numerical tools

Being system (7) strongly nonlinear, analytical solution is not known to exist. Slight changes of the parameters may cause topologically different solutions. Therefore, to analyze the system and to describe the oscillation structure of the bubble, one has to solve it numerically.

In the present study, system (7) was treated as an initial value problem (IVP). From a fixed initial condition, the differential equation system was integrated forward in time until the transient solution converged to an attractor. After the convergence of a solution, its characteristic properties were saved such as points of the Poincaré section, period, or maximum bubble radius [21]. This is a very common method to examine nonlinear systems in general, for details see e.g. [46–49]. The IVP solver was a 4th order Runge–Kutta scheme with 5th order embedded error estimation. In order to find all the relevant stable orbits, at each parameter set, 5 IVPs were solved with randomly chosen initial conditions.

The basic means to explore the topological structure of the attractors were pressure amplitude response curves, where the first coordinate of the Poincaré plane $P(y_1)$ was plotted versus the control parameter p_A at different equilibrium radii R_E. The number of the applied equilibrium radii R_E was 19 varied between 1 μm and 0.1 m, and distributed logarithmically. In each diagram, the pressure amplitude p_A was varied between 1 bar and 5 bar with 0.01 bar increment. From the series of such bifurcation curves, two dimensional bi-parametric plots (contour plots) were generated. In this $p_A - R_E$ plane, the color-coded period of the stable solutions were presented in order to efficiently show the evolution of the bifurcation structure.

3 Results

The computed pressure amplitude response curves and bi-parametric diagrams reveal the strong similarities between the bifurcation structures obtained at different equilibrium radii R_E, if the relative frequency ω_f is kept constant. In this section, we show few examples of these diagrams, and discus that how our results extend Behnia's findings [1].

3.1 Topological similarities of the bifurcation structures

Figure 1 shows eight pressure amplitude response curves at different equilibrium radii and two excitation frequencies. The series of Fig. 1a-d corresponds to relative frequency $\omega_f = 0.5$, while Fig. 1e-h to $\omega_f = 2$. The results suggest that the bifurcation structure is independent of the bubble radius approximately above $R_E = 5\,\mu$m. The main features of the two kinds of bifurcation structures are as follows.

At low frequency ($\omega_f = 0.5$), the initial period 1 orbit, which is emerged from the dimensionless equilibrium radius $y_{1,E} = 1$ of the unexcited system, undergoes a period doubling (PD) bifurcation near pressure amplitude $p_A = 1$ bar and becomes unstable. Here, a

narrow band of chaotic solutions also exists indicated by the scattered Poincaré points. The upper branch of the period 1 curve, appeared via a saddle–node (SN) bifurcation, exhibits Feigenbaum period doubling cascade transforming gradually into a large chaotic domain.

At the subharmonic resonant frequency ($\omega_f = 2$), the initial period 1 solution undergoes a PD bifurcation at very low pressure amplitude p_A. This is a well-known characteristic properties of nonlinear systems excited at frequency value two times their resonant frequency [36,50]. The emerged period 2 region exists approximately up to pressure amplitude $p_A = 3\,\text{bar}$. Meanwhile, a co-existing period 3 orbit appears via SN bifurcation and finishes in PD cascade. Above $p_A = 3.5\,\text{bar}$, the bifurcation structure alternates between periodic and chaotic windows.

At bubble size lower than $R_E = 5\,\mu\text{m}$, the topology becomes more simple. The bifurcation points are shifted towards higher pressure amplitudes, and the chaotic oscillations are almost disappeared, see Fig. 1d and h.

For a better visualisation of the evolution of the bifurcation structure, two bi-parametric plots were created at both relative frequency employing all the pressure amplitude response curves computed at the prescribed 19 number of bubble sizes (Fig. 2 and 3). Instead of the first component of the Poincaré section $P(y_1)$, here, the period of the found attractors is presented to be able to easily trace the bifurcation points. The results in the $p_A - R_E$ plane show clearly that there is no sharp threshold (in terms of bubble size R_E) for the conformity of the structure. The bifurcation points are gradually dislocated towards high pressure amplitudes with decreasing equilibrium bubble radius. Consequently, any threshold must be somehow an arbitrarily chosen value. Our choice, the previously prescribed $R_E = 5\,\mu\text{m}$, is highlighted by the red lines in Fig. 2 and 3.

A very similar observation was found by Behnia and his co-workers [1]. They stated that the bifurcation structure of the pressure amplitude response diagrams are strongly similar provided that $R_E\omega$ is kept constant. This condition is not exactly the same as ours (ω_f is constant). The relationship between them will be explained in more details in the next subsections. An important conclusion, however, have to be noticed here. Although Behnia provided no validity limit for their condition, Fig. 2 and 3 reveal that it is not universal.

3.2 The dimensionless equation system with constant $R_E\omega$

In this subsection, Behnia's condition is examined via dimensional analysis of system (7). For simplicity, let us define C as

$$C = \frac{R_E\omega}{2\pi}. \tag{20}$$

With constant C, parameters (10)-(14) read as follows:

$$p_{ref} = \rho_L C^2, \tag{21}$$

$$\mu_{ref} = c_L\rho_L R_E, \tag{22}$$

$$\mu^A_{ref} = c_L\rho_L C, \tag{23}$$

$$\mu^B_{ref} = c_L\rho_L \frac{C}{(2\pi)}, \tag{24}$$

and finally the Mach number at time τ is

$$M = \frac{y_2}{c_L}C. \tag{25}$$

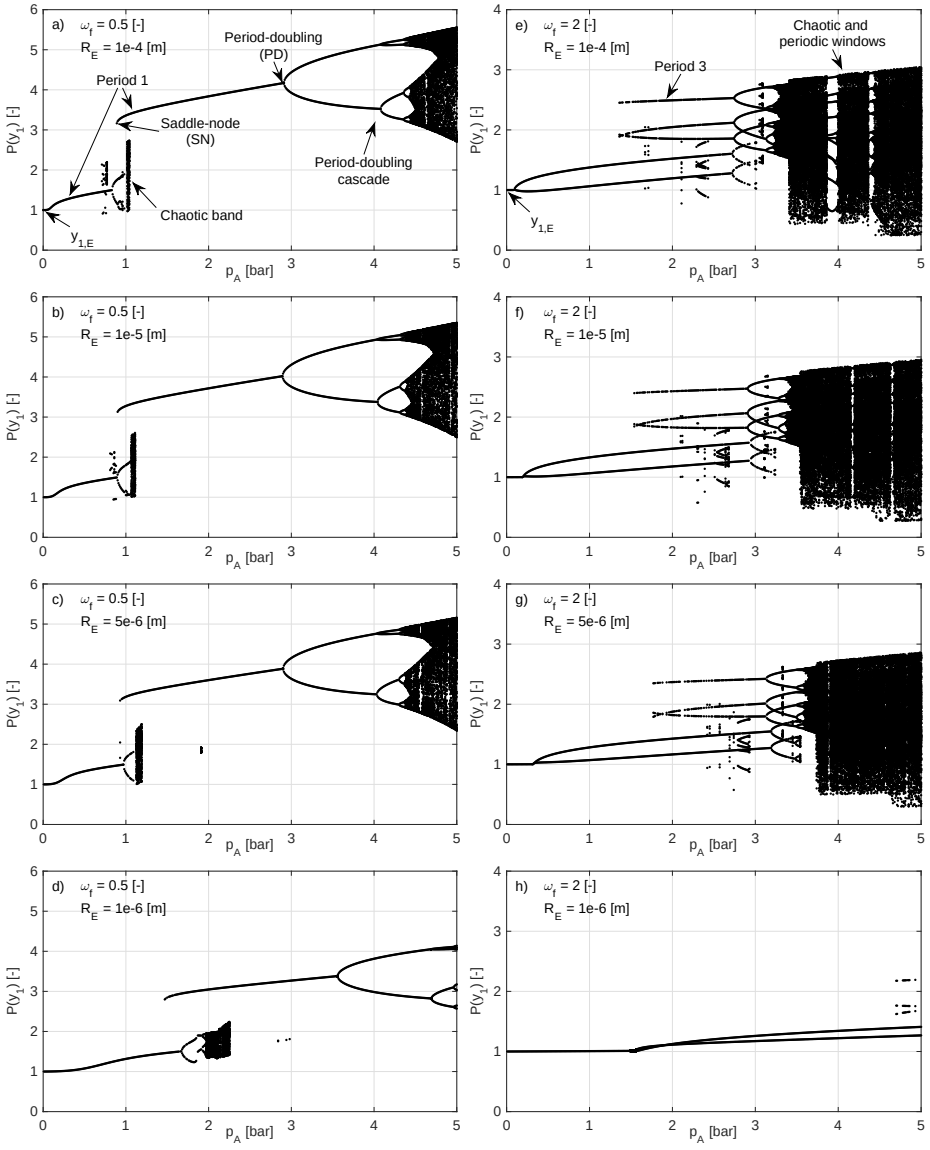

Fig. 1 Pressure amplitude response curves of the dimensionless bubble radius. at the different relative frequencies and equilibrium radii.

Equations (15)-(17) cannot be simplified further. The gas pressure p_G and liquid pressure p_L are still affected by the surface tension σ and the liquid dynamic viscosity μ_L. Due to the introduced dimensionless time τ, the pressure far away from the bubble $p_\infty(\tau)$ no longer depends on ω, but still on the pressure amplitude p_A.

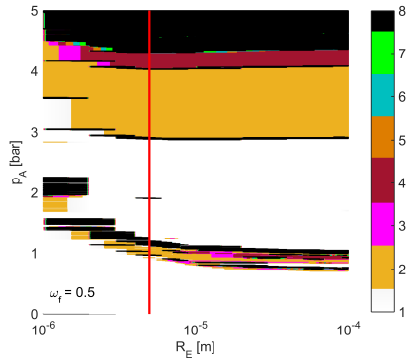

Fig. 2 Bi-parametric bifurcation structure of the bubble oscillator at relative frequency $\omega_f = 0.5$. The colorbar represents the highest period of the found attractors in the $p_A - R_E$ plane.

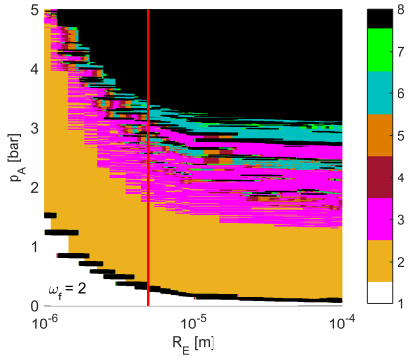

Fig. 3 Bi-parametric bifurcation structure of the bubble oscillator at relative frequency $\omega_f = 2$. The colorbar represents the highest period of the found attractors in the $p_A - R_E$ plane.

With the above listed equations, the numerator (8) and the denominator (9) become

$$\begin{aligned} N = & \frac{p_G + p_V}{C^2 \rho_L} - \frac{1}{y_1 C \rho_L} \frac{2\sigma}{R_E} - \frac{y_2}{y_1 C} \frac{4\mu_L}{\rho_L R_E} \\ & + \frac{y_2}{y_1 c_L C \rho_L} \left(p_G (1 - 3n) - p_\infty(\tau) + p_V \right) \\ & - \frac{1}{2\pi} \frac{p_A \cos(2\pi\tau)}{c_L C \rho_L} - \left(3 - \frac{y_2}{c_L} C \right) \frac{1}{2} \frac{y_2^2}{y_1}, \end{aligned} \tag{26}$$

and

$$D = 1 - \frac{y_2}{c_L} C + \frac{1}{y_1 c_L} \frac{4\mu_L}{\rho_L R_E}, \tag{27}$$

respectively. In the expressions N and D (including p_G and p_L), there are only two kinds of parameters which are not constant when C is constant, namely,

$$\frac{2\sigma}{R_E} \tag{28}$$

and

$$\frac{4\mu_L}{\rho_L R_E}. \tag{29}$$

It follows that when the dynamic viscosity of the liquid μ_L and the surface tension σ are negligible, the bifurcation structure does not change when $C = R_E\omega/2\pi$ is kept constant. This gives a precise explanation on why the bifurcation structures are similar on a wide range of parameters in the study of Behnia [1]. But the influences of σ and μ_L with respect to the equilibrium bubble radius R_E have to be still clarified.

3.3 The linear resonance frequency of the bubble

Before proceeding with the discussion of the validity threshold in terms of R_E, let us determine the relationship between the conditions of Behnia

$$R_E\omega = \text{constant} \tag{30}$$

and the present study

$$\omega_f = \frac{\omega}{\omega_0} = \text{constant}. \tag{31}$$

The linear resonant frequency ω_0 of the system, Eq. (19), multiplied by R_E is

$$\omega_0 R_E = \sqrt{\frac{3n(P_\infty - p_v)}{\rho_L} + \frac{2(3n-1)\sigma}{\rho_L R_E} - \frac{4\mu_L^2}{\rho_L^2 R_E^2}}, \tag{32}$$

which can be further simplified to

$$\omega_0 R_E = \sqrt{\frac{3n(P_\infty - p_v)}{\rho_L}} \approx \sqrt{\frac{3nP_\infty}{\rho_L}} \tag{33}$$

if the effects of the surface tension σ and dynamic liquid viscosity μ_L are neglected. Observe that these assumptions are exactly the same as in case of Behnia's condition (30), see also Eqs. (28) and (29). The resonant frequency ω_0 in Equation (33) is also known as the Minnaert frequency [51]. With the material properties summarized in Table 1, the relation $\omega_0 R_E \approx 20.1\,\mathrm{m/s}$ holds. Now, it is clear that if $R_E\omega$ is constant than the relative frequency

$$\omega_f = \frac{\omega}{\omega_0} = \frac{R_E\omega}{R_E\omega_0} \tag{34}$$

is constant as well, implying that conditions (30) and (31) are identical when $\sigma, \mu \to 0$.

The validity range of these two conditions is examined through the analysis of the linear resonant frequency (19). Figure 4 shows how the two terms of Eqs. (28) and (29) effect ω_0 in a wide range of equilibrium radius on a logarithmic scale. The black line is the full equation, the blue line represents the case when μ_L is neglected, and the red line shows the Minnaert frequency, when both μ_L and σ are zero.

For equilibrium radii larger than about $R_E = 0.05\,\mu\mathrm{m}$, there is no significant difference between the black and the blue line, which means that in this range of the bubble size, the effect of μ_L is negligible, see Fig. 4b. When both terms related to σ and μ_L are neglected (red solid line), the linear resonance frequency starts to differ from the black line for equilibrium radii smaller than about $R_E = 5\,\mu\mathrm{m}$. Since the effect of the liquid dynamic viscosity is not significant for bubble sizes larger than $R_E = 0.05\,\mu\mathrm{m}$, here, the difference between the

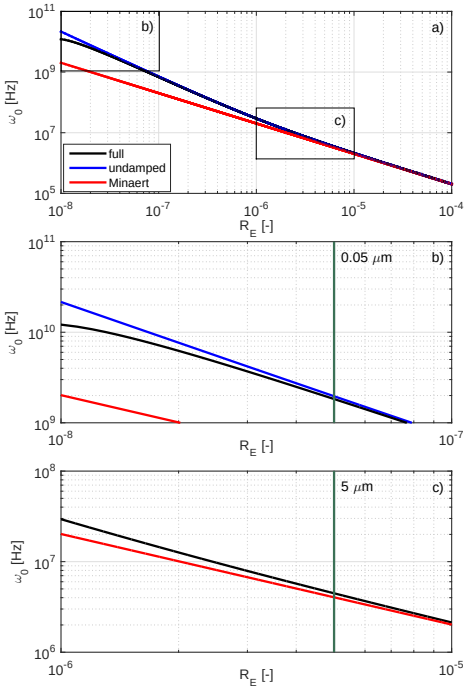

Fig. 4 The linear resonance frequency ω_0 of the bubble as the function of the equilibrium radius R_E. When both the damping μ_L and the surface tension σ are taken into account, its evolution is shown by the black line. The undamped eigenfrequency is shown by the blue line, and the red line shows when both μ_L and σ is neglected (Minnaert frequency [51]).

black and the red lines is caused solely by the surface tension. These threshold values for the bubble sizes are rather arbitrarily, as it is already stated before. But the findings are in very good accordance with the results obtained by analyzing the bifurcation structure itself (Fig. 1).

Although the bubble size distribution of a bubble cluster in water is highly frequency dependent, it is possible to roughly estimate a typical bubble size, which is approximately between $R_E = 1\,\mu$m and $R_E = 5\,\mu$m [52–55]. During the radial pulsation of the bubbles, they can grow by rectified diffusion [56–58], but the experimental and numerical results have shown that their size cannot exceed approximately $R_E = 10\,\mu$m due to the shape instability [59,60]. Therefore, in water, the effect of liquid viscosity μ_L can definitely be negligible. However, the observed bubble sizes are exactly in the range where the effect of surface tension σ becomes important implying that the similarity in the bifurcation structure shall be hard to verify experimentally.

Increasing the liquid viscosity, the shape stability can be increased significantly. Hegedűs et. al. [61] observed stable bubble oscillations even at equilibrium bubble radius $R_E = 0.1\,$mm in highly viscous glycerine. In case of very high viscosity, however, the effect of μ_L can become dominant, which may cause much higher threshold value for conditions (28) and (29) than $R_E = 5\,\mu$m. This implication is supported by the observation of Hegedűs and Klapcsik [23], who found overdamped bubble oscillations in pure glycerine with liquid temperature smaller than $T_\infty = 27\,^\circ$C. This means negative value under the root in Eq. (19). An intermediate solution can be the application of water–glycerine mixture, where the viscosity

is high enough to increase the shape stability but not as high as to become important in the calculation of the linear resonant frequency.

4 Conclusion

In the present study, the characterization of the bifurcation structure of a harmonically excited, single spherical bubble was presented. The used bubble oscillator was the Keller-Miksis equation, and the liquid medium was water. Results show in accordance with Behnia et al. [1] that when the value of $R_E\omega$ is kept constant, the bifurcation structure of the pressure amplitude response curves are strongly similar. Examining the bubble oscillator analytically and numerically, we found that this condition is not universal, but it depends on the liquid dynamic viscosity μ_L and the surface tension σ. In water, the effect of the viscosity μ_L is negligible, and the surface tension σ plays significant role only if the equilibrium radius is smaller than approximately $R_E = 5\,\mu$m.

Acknowledgements The research described in this paper was supported by the Hungarian Scientific Research Fund – OTKA, Grant No. K81621.

This paper was supported by the János Bolyai Research Scholarship of the Hungarian Academy of Sciences.

References

1. S. Behnia, A.J. Sojahrood, W. Soltanpoor, L. Sarkhosh, Ultrasonics **49**(8), 605 (2009)
2. T.G. Leighton, *The acoustic bubble* (Academic press, London, 2012)
3. R. Mettin, in *Oscillations, Waves and Interactions: Sixty Years Drittes Physikalisches Institut ; a Festschrift* (Universitätsverlag Göttingen, Göttingen, Germany, 2007)
4. R. Mettin, in *Bubble and Particle Dynamics in Acoustic Fields: Modern Trends and Applications* (Research Signpost, Trivandrum, Kerala, India, 2005)
5. R. Mettin, C. Cairós, A. Troia, Ultrason. Sonochem. **25**, 24 (2015)
6. T.J. Mason, Ultrason. Sonochem. **25**, 89 (2015)
7. L. Stricker, D. Lohse, Ultrason. Sonochem. **21**(1), 336 (2014)
8. M. Rahimi, S. Safari, M. Faryadi, N. Moradi, Chem. Eng. Process. **78**, 17 (2014)
9. S. Khanna, S. Chakma, V.S. Moholkar, Chem. Eng. Sci. **100**, 137 (2013)
10. P. Kanthale, M. Ashokkumar, F. Grieser, Ultrason. Sonochem. **15**(2), 143 (2008)
11. Y. Iida, T. Tuziuti, K. Yasui, A. Towata, T. Kozuka, Innov. Food Sci. Emerg. **9**(2), 140 (2008)
12. D. Knorr, M. Zenker, V. Heinz, D.U. Lee, Trends Sci. Tech. **15**(5), 261 (2004)
13. R. Seshadri, J. Weiss, G.J. Hulbert, J. Mount, Food Hydrocolloids **17**(2), 191 (2003)
14. S. Mitragotri, Nat. Rev. Drug. Discov. **4**, 255 (2005)
15. Z. Xu, A. Ludomirsky, L.Y. Eun, T.L. Hall, B.C. Tran, J.B. Fowlkes, C.A. Cain, IEEE Trans. Ultrason. Ferroelectr. Freq. Control **51**(6), 726 (2004)
16. J.E. Kennedy, G.R.t. Haar, D. Cranston, Brit. J. Radiol. **76**(909), 590 (2003)
17. C.H. Chaussy, W. Brendel, E. Schmiedt, Lancet **316**(8207), 1265 (1980)
18. W. Lauterborn, T. Kurz, Rep. Prog. Phys. **73**(10), 106501 (2010)
19. Z.C. Feng, L.G. Leal, Annu. Rev. Fluid. Mech. **29**(1), 201 (1997)
20. M.S. Plesset, A. Prosperetti, Annu. Rev. Fluid Mech. **9**(1), 145 (1977)
21. R. Varga, G. Paál, Chaos Solitons Fract. **76**, 56 (2015)
22. A.J. Sojahrood, O. Falou, R. Earl, R. Karshafian, M.C. Kolios, Nonlinear Dyn. **80**(1-2), 889 (2015)
23. F. Hegedűs, K. Klapcsik, Ultrason. Sonochem. **27**, 153 (2015)
24. F. Hegedűs, Ultrasonics **54**(4), 1113 (2014)
25. S. Behnia, H. Zahir, M. Yahyavi, A. Barzegar, F. Mobadersani, Nonlinear Dyn. **72**(3), 561 (2013)
26. S. Behnia, F. Mobadersani, M. Yahyavi, A. Rezavand, Nonlinear Dyn. **74**(3), 559 (2013)
27. F. Hegedűs, C. Hős, L. Kullmann, IMA J. Appl. Math. **78**(6), 1179 (2013)
28. A.J. Sojahrood, M.C. Kolios, Phys. Lett. A **376**(33), 2222 (2012)
29. F. Hegedűs, L. Kullmann, Period. Polytech. Mech. Eng. **56**(2), 125 (2012)

30. S. Behnia, A.J. Sojahrood, W. Soltanpoor, O. Jahanbakhsh, Chaos Solitons Fract. **41**(2), 818 (2009)
31. S. Behnia, A.J. Sojahrood, W. Soltanpoor, O. Jahanbakhsh, Ultrason. Sonochem. **16**(4), 502 (2009)
32. E.A. Brujan, Acta Acust. United Acust. **95**(2), 241 (2009)
33. G. Simon, P. Cvitanovic, M.T. Levinsen, I. Csabai, A. Horvth, Nonlinearity **15**(1), 25 (2002)
34. U. Parlitz, V. Englisch, C. Scheffczyk, W. Lauterborn, J. Acoust. Soc. Am. **88**(2), 1061 (1990)
35. W. Lauterborn, U. Parlitz, J. Acoust. Soc. Am. **84**(6), 1975 (1988)
36. W. Lauterborn, J. Acoust. Soc. Am. **59**(2), 283 (1976)
37. T. Kurz, W. Lauterborn, Phys. Rev. A **37**, 1029 (1988)
38. C. Bonatto, J.A.C. Gallas, Y. Ueda, Phys. Rev. E **77**(2), 026217 (2008)
39. S.Y. Kim, Int. J. Mod. Phys. B **14**(17), 1801 (2000)
40. R. Gilmore, J.W.L. McCallum, Phys. Rev. E **51**, 935 (1995)
41. J. Kozłowski, U. Parlitz, W. Lauterborn, Phys. Rev. E **51**(3), 1861 (1995)
42. C. Scheffczyk, U. Parlitz, T. Kurz, W. Knop, W. Lauterborn, Phys. Rev. A **43**(12), 6495 (1991)
43. J.B. Keller, M. Miksis, J. Acoust. Soc. Am. **68**(2), 628 (1980)
44. L. Haar, J.S. Gallagher, G.S. Kell, *NBS/NRC Wasserdampftafeln* (Springer, Berlin, 1988)
45. C.E. Brennen, *Cavitation and Bubble Dynamics* (Oxford University Press, New York, 1995)
46. G. Závodszky, G. Károlyi, G. Paál, J. Theor. Biol. **368**, 95 (2015)
47. C.J. Hős, A.R. Champneys, K. Paul, M. McNeely, J. Loss Prevent. Proc. **36**, 1 (2015)
48. C. Hős, A.R. Champneys, Physica D **241**(22), 2068 (2012)
49. C. Hős, A.R. Champneys, L. Kullmann, IMA J. Appl. Math. **68**(2), 205 (2003)
50. A. Prosperetti, J. Acoust. Soc. Am. **56**(3), 878 (1974)
51. M. Minnaert, Philos. Mag. **16**(104), 235 (1933)
52. A. Brotchie, F. Grieser, M. Ashokkumar, Phys. Rev. Lett. **102**(8), 084302 (2009)
53. J. Lee, M. Ashokkumar, S. Kentish, F. Grieser, J. Am. Chem. Soc. **127**(48), 16810 (2005)
54. W.S. Chen, T.J. Matula, L.A. Crum, Ultrasound Med. Biol. **28**(6), 793803 (2002)
55. F. Burdin, N.A. Tsochatzidis, G. P., H. Wilhelm, A. M.and Delmas, Ultrason. Sonochem. **6**(12), 43 (1999)
56. O. Louisnard, F. Gomez, Phys. Rev. E **67**(3), 036610 (2003)
57. M.M. Fyrillas, A.J. Szeri, J. Fluid Mech. **277**, 381 (1994)
58. L.A. Crum, Ultrasonics **2**(5), 215 (1984)
59. P. Koch, T. Kurz, U. Parlitz, W. Lauterborn, J. Acoust. Soc. Am. **130**(5), 3370 (2011)
60. J. Holzfuss, Phys. Rev. E **77**(6), 066309 (2008)
61. F. Hegedűs, S. Koch, W. Garen, Z. Pandula, G. Paál, L. Kullmann, U. Teubner, Int. J. Heat Fluid Fl. **42**, 200 (2013)